Desalination 557 (2023) 116580

Contents lists available at ScienceDirect

Desalination

journal homepage: www.elsevier.com/locate/desal

Theory for salt transport in charged reverse osmosis membranes: Novel analytical equations for desalination performance and experimental validation

P.M. Biesheuvel [a], S.B. Rutten [a,b], I.I. Ryzhkov [c,d], S. Porada [a,e], M. Elimelech [f,*]

[a] Wetsus, European Centre of Excellence for Sustainable Water Technology, The Netherlands
[b] Membrane Science & Technology, University of Twente, The Netherlands
[c] Institute of Computational Modelling SB RAS, Akademgorodok 50, 660036 Krasnoyarsk, Russia
[d] Siberian Federal University, Svobodny 79, 660041 Krasnoyarsk, Russia
[e] Department of Process Engineering and Technology of Polymer and Carbon Materials, Wroclaw University of Science and Technology, Wyb. St. Wyspiańskiego 27, 50-370 Wrocław, Poland
[f] Department of Chemical and Environmental Engineering, Yale University, USA

HIGHLIGHTS

- Novel equation for salt transport in reverse osmosis (RO) interpolates between the limits of high and low membrane charge.
- Physical meaning to the phenomenological parameters in the classical Spiegler-Kedem (SK) equations.
- Extension of these SK model equations to 1:1 electrolyte solutions.
- Proposed protocol for accurate and robust testing of RO membranes to derive intrinsic membrane parameters.

ARTICLE INFO

Keywords:
Desalination
Reverse osmosis
Salt permeability
Water permeability
Ion transport
Solution-friction model

ABSTRACT

Reverse osmosis (RO) is one of the most successful membrane technologies for desalination and contaminant removal from water. RO is applied globally, and can be used for both small- and large-scale applications. To characterize membrane performance, standard testing uses membrane coupons and a NaCl solution in a labscale setup under controlled conditions. Ideally, experiments are done for a range of applied hydrostatic pressures and salt concentrations, with water flux and salt rejection measured in each experiment. This full dataset can then be checked for internal consistency, and all these data must then be described by a comprehensive theoretical framework, i.e., we need an appropriate set of equations to parametrize these data. Parameters derived from this procedure, such as water and salt permeability, can then be compared to those obtained in other studies, for other membranes, salts, or temperatures. If this theory indeed correctly describes data for water flux and salt flux, it can also be applied in larger scale models for RO modules and combinations of modules, which are the basis of engineering design and economic optimization. Herein, we present a novel equation for salt flux that we derive from the full solution-friction (SF) theory. This equation interpolates between an equation for neutral membranes on the one hand, and an equation for highly-charged membranes on the other hand, and thus it is more generally applicable. We apply this new equation to several datasets of seawater RO membranes, and we propose an accurate method to compare the salt permeability of different membranes.

1. Introduction

Reverse osmosis (RO) is a membrane technology that is globally applied to remove salts and organic contaminants from water. In this paper, we focus on salt removal, and assume that the water only contains monovalent anions and cations [1–3]. In RO, water is pushed through a highly selective membrane that rejects most of the salt ions. Therefore, the permeate, or freshwater, has a salt concentration orders of

* Corresponding author.
E-mail address: menachem.elimelech@yale.edu (M. Elimelech).

https://doi.org/10.1016/j.desal.2023.116580
Received 22 January 2023; Received in revised form 3 March 2023; Accepted 17 March 2023
Available online 7 April 2023
0011-9164/© 2023 Elsevier B.V. All rights reserved.

magnitude lower than in the feedwater. Membranes for RO are either classified as suitable for the desalination of seawater (SW) or for brackish water (BW). Membranes for BW are more porous and less selective, and require less pressure. A related technology is nanofiltration (NF), which uses even more open membranes and lower pressures, but NF membranes do not have a high rejection for monovalent salts.

The development of a correct theoretical description for the transport of water and salts across RO membranes is an important scientific challenge with great technological relevance. We need a good theory because then we can summarize or 'parametrize' with a few parameters the performance of a certain membrane that we test at many applied pressures and feedwater salt concentrations. The parameters that we derive from comparing the theory to this full dataset can then be compared to those derived in other studies, either for the same membrane but with different protocols, or at different temperatures, or for different salts. These parameters can also be compared between different membranes, or between different coupons from what is marketed as the same membrane. If the parametrization is successful (i.e., the theory fits the data), the theory is accurate and can then be used in models of a full RO module. These are models that are used in engineering studies and economic optimization. If the theory fits data for single salt solutions, we can also have confidence that we are in the right direction for the development of models for multicomponent solutions. Such models are required to describe the desalination of water from real sources.

In this paper, we present a novel equation for salt flux and salt rejection, which interpolates between two limits. These limits are on the one hand an equation for uncharged membranes and neutral solutes, which is generally referred to as the solution-diffusion (SD) model [4–6], and on the other hand an equation for membranes that are highly charged, which is the good co-ion exclusion (GCE) limit [2,7]. The new equation is derived from the full solution-friction (SF) theory [1–3] and can be applied to the entire range between these two limits. So it can be used to describe datasets where an effect of membrane charge is absent, and thus feed salt concentration has no effect on rejection (when comparing results at the same transmembrane water flux), and it can also be used for datasets where membrane charge plays a relevant role and thus rejection depends on feed salinity. This theory describes water flux and salt flux with four parameters: water permeability A, a transport factor P, a charge factor C, and a coefficient for the upstream diffusion boundary layer (DBL, i.e., the effect of concentration polarization, CP), k_{dbl}. We apply these equations to several datasets of salt rejection and water flux for seawater RO membranes, and we describe an accurate method how to derive salt permeability information that can be compared between membranes.

2. Theory

In this section, we derive a semi-analytical equation for the transmembrane salt flux based on the full SF theory, valid in the entire range from RO membranes being uncharged to highly charged. The resulting equation parametrizes membrane performance with two parameters, P and C, while the upstream boundary layer is described by a mass transfer coefficient k_{dbl}. The starting point is the extended Nernst-Planck equation evaluated inside the membrane, combining convection, diffusion, and electromigration as driving forces for the flux J_i of an ion, which leads to [1–3]

$$J_i = K_{\mathrm{f},i} c_i v_{\mathrm{w}} - K_{\mathrm{f},i} k_{\mathrm{m},i} \left(\frac{\partial c_i}{\partial x} + z_i c_i \frac{\partial \phi}{\partial x} \right) \tag{1}$$

where v_{w} is the transmembrane water flux in $\mathrm{m^3/m^2/s}$, i.e., it is a velocity with unit m/s (or equivalently it can be expressed in $\mathrm{L/m^2/h}$, which is abbreviated as LMH), the ion mass transfer coefficient is $k_{\mathrm{m},i} = \varepsilon D_i / L_{\mathrm{m}}$ (also with unit m/s or LMH), and the dimensionless coordinate is $x = \bar{x}/L_{\mathrm{m}}$, see List of Symbols for an overview of all parameters. The variable ε is a reduction factor due to the porosity and tortuosity of the porous medium, and $\bar{x}$ is the coordinate across a membrane of thickness L_{m}. The friction factor $K_{\mathrm{f},i}$ describes the importance of friction of ions with the membrane structure (the matrix) versus friction of ions with the water, with $K_{\mathrm{f},i} = 1$ referring to no ion-matrix friction and $K_{\mathrm{f},i} \to 0$ indicating that friction of ions with the membrane structure is much more important than friction with the water in the pores. The diffusion coefficient D_i is the inverse of an ion-water friction in the absence of the membrane structure, and the dimensionless electrical potential is ϕ. This potential ϕ is the dimensional electrical potential V scaled by RT/F, where R is the universal gas constant, T is the temperature, and F is Faraday constant.

We now consider a 1:1 salt with a monovalent anion and a monovalent cation. We assume that in the membrane the two ions have the same $K_{\mathrm{f},i}$ and $k_{\mathrm{m},i}$, and thus we leave out index i. In RO there is zero current through the membrane, thus $J_{\mathrm{ch}} = J_+ - J_- = 0$, while at each position in the membrane we assume charge neutrality, $c_+ - c_- + X = 0$, with X being a membrane charge density that is expressed as a concentration, a number that can be positive and negative. We can then derive for the salt flux J_{s} [2]

$$J_{\mathrm{s}} = \frac{1}{2} K_{\mathrm{f}} \left(v_{\mathrm{w}} \left(c_{\mathrm{T,m}} - \frac{X^2}{c_{\mathrm{T,m}}} \right) - k_{\mathrm{m}} \frac{\partial c_{\mathrm{T,m}}}{\partial x} \right) \tag{2}$$

where the total ions concentration at any position x in the membrane is $c_{\mathrm{T,m}} = c_+ + c_-$. A detailed derivation is provided in the Supplementary material. All concentrations are defined per unit volume of the water-filled pores. On the two outsides of the membrane, the two values of $c_{\mathrm{T,m}}$ depend on the membrane charge density, X, the outside salt concentration, c, and the partition coefficient, Φ, that includes all effects except for those related to charge neutrality (Donnan), according to [1–3]

$$c_{\mathrm{T,m}} = \sqrt{X^2 + (2\Phi c)^2}. \tag{3}$$

Concentration c is either the interface concentration, c_{int}, which is the salt concentration just outside the membrane on the upstream side (sometimes called membrane concentration), or it is the concentration on the permeate side, c_{p}. The interface concentration c_{int} is different from the bulk concentration in the upstream (feed) channel some distance away from the membrane because of concentration polarization (the effect of the DBL), which we discuss further on. The partition coefficient Φ is the geometric mean partition coefficient of Φ_i of the two ions, $\Phi = \sqrt{\Phi_+ \Phi_-}$.

Eq. (2) can be analytically integrated across the membrane from left to right, resulting in an implicit relation between salt flux J_{s} and $c_{\mathrm{T,m}}$ on the two outsides. The derivation is provided in Supplementary material. Eq. (2) can also be solved numerically, and the most robust method is then to first implement Eq. (2) in a mass balance, which for steady state and a single coordinate x implies that $\partial J_{\mathrm{s}}/\partial x = 0$, resulting in

$$\frac{v_{\mathrm{w}}}{k_{\mathrm{m}}} \left(1 + \frac{X^2}{c_{\mathrm{T,m}}^2} \right) \frac{\partial c_{\mathrm{T,m}}}{\partial x} - \frac{\partial^2 c_{\mathrm{T,m}}}{\partial x^2} = 0. \tag{4}$$

This equation can be numerically solved at gridpoints 1 ... $n-1$ that relate to equidistant positions across the membrane thickness (with positions 0 and n being the outsides of the membrane), and combined with an integration of Eq. (2), which is

$$J = \frac{1}{2} K_{\mathrm{f}} \left(v_{\mathrm{w}} \left(\langle c_{\mathrm{T,m}} \rangle - X^2 / \langle c_{\mathrm{T,m}} \rangle^{\dagger} \right) + k_{\mathrm{m}} \Delta c_{\mathrm{T,m}} \right) \tag{5}$$

where $\langle c_{\mathrm{T,m}} \rangle = \int_0^1 c_{\mathrm{T,m}} \mathrm{d}x$ and $1/\langle c_{\mathrm{T,m}} \rangle^{\dagger} = \int_0^1 1/c_{\mathrm{T,m}} \mathrm{d}x$, and $\Delta c_{\mathrm{T,m}} = c_{\mathrm{T,m}}|_{x=0} - c_{\mathrm{T,m}}|_{x=1}$, where positions 0 and 1 refer to just in the membrane on the upstream and downstream side. These two integrations can be numerically solved based on the Trapezoid rule,

$\int y\,dx \approx 1/(2n)\ \sum_{i=1\ldots n}(y_{i-1}+y_i)$.

It is interesting to implement Eq. (3) directly in Eq. (2), and then we have a salt flux as function of a virtual concentration c that gradually changes with x from the value c_{int} on the upstream (feed) side to c_p on the downstream (permeate) side. Only on the edges, is c 'real', namely equal to the outside concentrations there. In between these positions c is only a theoretical concentration, which can be recalculated at each position to $c_{T,m}$ with Eq. (3), and after that anion and cation concentrations can also be calculated. For instance, the counterion concentration (the ion of opposite sign of charge as that of the membrane) is $c_{ct} = \frac{1}{2}\left(|X|+c_{T,m}\right)$. This modified salt flux equation is

$$J_s\sqrt{\left(\frac{C}{c}\right)^2+1} = -P\frac{\partial c}{\partial x}+(1-\sigma)cv_w \tag{6}$$

where the charge factor C is given by $C = |X|/2\Phi$. The entire right side is the same as in classical versions of the SF model for neutral solutes originally developed by Spiegler and Kedem in 1966 [8], see also refs. [9–12]. Thus, now that we consider a 1:1 salt and a charged membrane, the only addition is the extra factor on the left. The transport factor $P = K_f\Phi k_m$ is also denoted in the literature as P_s or ω, or replaced by $(1-\sigma)k_m$. The reflection coefficient, σ, is $\sigma = 1 - K_f\Phi$. Thus, Eq. (6) is an extension of the Spiegler-Kedem equation, which was derived for an uncharged membrane, to the case of a charged membrane and a 1:1 salt solution. Also Hoffer and Kedem [13] derive an equation for charged membranes, but their Eq. (16) is different from our result. If membrane charge is zero, then C is zero, and Eq. (6) simplifies to the expression for neutral membranes [8–10]. In that case, the analytical solution is the Hertz equation [3], but for $X \neq 0$, Eq. (6) does not have an analytical solution.

The above equations are generally applicable to describe steady-state transport of salt across a membrane, for any kind of condition or geometry outside the membrane, and for low and high water recovery. For instance, the equations above can be solved at each position in a flow channel where on both sides of the membrane we solve the 1D or 2D velocity and concentration profiles. Except for Eqs. (8)–(10) and Eq. (16), the equations from this point onward assume a low water recovery, such that on the upstream side the concentration does not change much through a flow channel between entrance and exit of a module. In that case the permeate concentration c_p relates to salt flux and water flux by $c_p = J_s/v_w$. This condition generally applies when a small coupon is tested in a cross-flow geometry, and also applies to a 'dead end' experiment, in which water is pushed through a membrane from a pressurized batch of feedwater without crossflow. We refer to this limit as 'low water recovery' or 'dead end (condition/experiment)'. Combining this low water recovery limit with Eq. (6) we obtain

$$\frac{\partial c}{\partial x} = \frac{v_w}{P}\left((1-\sigma)c - c_p\sqrt{\left(\frac{C}{c}\right)^2+1}\right) \tag{7}$$

which for an uncharged membrane, when $C = 0$, simplifies to Eq. (32) in ref. [12], Eq. (1) in ref. [15], and Eq. (1) in ref. [16]. Thus, Eq. (7) is an extension of that equation to the case of a charged membrane and a 1:1 salt.

For RO membranes it is assumed that convection is not a significant contribution to salt transport, and thus the term linear in v_w in Eqs. (2) and (6) can be neglected. Integration across the membrane thickness then results in

$$J_s = P\left(\sqrt{C^2+c_{int}^2}-\sqrt{C^2+c_p^2}\right) \tag{8}$$

which is generally applicable, for instance, at each position in a full 2D transport model of a membrane module. Eq. (8) can be combined with a general equation for the DBL, given by (see [11]).

$$c_{int} = c_f\ e^{Pe_{dbl}} - \left(e^{Pe_{dbl}}-1\right)\frac{J_s}{v_w} \tag{9}$$

where $Pe_{dbl} = v_w/k_{dbl}$. When $J_s/v_w \ll c_f$, Eq. (9) simplifies to

$$c_{int} = c_f e^{Pe_{dbl}} = c_f\exp(v_w/k_{dbl}). \tag{10}$$

The above equations have c_f as input, as in an experiment where the solution outside the DBL is continuously refreshed with a solution of concentration c_f. In a more general case, where the concentration just outside the DBL is position- and time-dependent, i.e., $c(z,t)$, then this latter, general notation is used to replace c_f in the equations in this section.

We now continue and describe an experiment at low water recovery, and thus the feed concentration, c_f, is used as a fixed concentration just outside the DBL. We assume a very good salt rejection, $c_p \ll c_f$, and thus Eq. (10) can be used to describe the DBL (CP layer). Without further assumptions salt rejection is then given by

$$R = 1-\frac{c_p}{c_f} = 1-\frac{P}{v_w}\left(\sqrt{\left(\frac{C}{c_f}\right)^2+\exp\left(2\frac{v_w}{k_{dbl}}\right)}-\frac{C}{c_f}\right) \tag{11}$$

where we again use the expression $J_s = v_w c_p$, which is valid for an experiment at low water recovery. Eq. (11) is the general new equation for salt rejection that we will use in the analysis in the next section. When C/c_f is low enough, which occurs when the membrane has no charge or not much, or if c_f is high enough, rejection is given by

$$R = 1-\frac{B}{v_w}\exp\left(\frac{v_w}{k_{dbl}}\right) \tag{12}$$

where we made the replacement $P \to B$, i.e., in this limit P is the same as the salt permeability B. In this case, rejection is independent of the charge parameter C and independent of feed concentration c_f. This limiting equation, in which membrane charge plays no role, is also used in the SD model. In the SD model, salt flux is given by the expression $J = B\left(c_{int}-c_p\right)$, and when the SD model is valid, we have $P = B$. Note that the equations in this section, from Eq. (11) above, to Eq. (14) below, all assume a very high rejection. For an uncharged membrane the generalization of Eq. (12) to allow for any value of rejection is $R = \left(1+B\exp(v_w/k_{dbl})/v_w\right)^{-1}$ [14].

Irrespective of whether a membrane is charged or not, we can use Eq. (12) to derive (measure) an *observed* salt permeability, B_{obs}, for any membrane and any condition, though this is most useful when rejection is high, and when the model for the CP-layer is valid, with a constant value of k_{dbl}. For an uncharged membrane, this B_{obs} is independent of c_{int} and is then the salt permeability, B. However, if many data of one membrane for B_{obs} follow a mastercurve that shows a dependence on c_{int}, this is an indication that the membrane is charged. How B_{obs} will depend on c_{int} can be derived from combining Eqs. (10)–(12), which then results in

$$B_{obs} = P\left(\sqrt{\left(\frac{C}{c_{int}}\right)^2+1}-\frac{C}{c_{int}}\right) \tag{13}$$

where c_{int} is given by Eq. (10).

It may not be so obvious, but B_{obs} increases with increasing c_{int}, first linearly at low c_{int}, until $c_{int} \sim C$, and then levelling off to P when $c_{int}/C \gtrsim 10$. That B_{obs} increases with an increase in the upstream salt concentration is a very common observation in NF [15–21] and has also been reported for RO membranes [1,22,23]. However, for RO it is also reported that B is independent of c_f [24]. It is relevant first of all to see if the data for B_{obs} for a certain membrane fall on a common 'mastercurve' because this is an indication that the theory discussed in this paper suffices. Because if they do not, then we have to consider corrections to the theory, which can relate to the CP-layer, the role of convection, or a

dependence of transport parameters or membrane charge on salt concentration.

Instead of the membrane having a low to zero charge, the opposite limit is that the charge factor C is high relative to c_f, and series expansion of Eq. (11) for $1/C \to 0$ results in a simplified equation for the good coion exclusion (GCE) limit, which is [2,3]

$$R = 1 - RTB'\frac{c_f}{v_w}\exp\left(\frac{2v_w}{k_{dbl}}\right) \tag{14}$$

where $B' = K_f k_m \Phi^2/RT|X|$, a factor that is also identified in ref. [7]. Thus, Eq. (11) interpolates between the zero-charge limit, Eq. (12), and the high-charge limit, Eq. (14).

As we will discuss in the next section, parameters C, P, and k_{dbl} can be derived when we compare calculations based on Eq. (11) with data from a large enough dataset. This analysis is made easier if in this process we construct three plots such as in Fig. 1, where we plot all data for B_{obs} versus c_{int}, rejection R versus water flux v_w, and v_w versus pressure difference $\Delta P^{h,\infty}$. All these plots contain data from experiments at several applied pressures and feed salt concentrations c_f. We vary the parameters A, C, P, and k_{dbl}, until all data are described by their corresponding theoretical lines in an optimal fashion.

For the relationship between transmembrane water flux and pressure, SF theory predicts

$$v_w = A\left(\Delta P^{h,\infty} - \sigma'\Delta\Pi\right) \tag{15}$$

where $\Delta P^{h,\infty}$ is the pressure difference between feed and permeate, σ' a reflection coefficient for charged membranes, and the osmotic pressure difference $\Delta\Pi$ is that between position 'int' and permeate. SF theory predicts that water permeability A is a function of solute concentrations in the membrane, but when water-membrane friction is dominant (over water-solute friction) this effect is not large, so in this work we use A as a constant factor not dependent on c_f. The reflection coefficient σ' is given by $\sigma' = 1 - (1-\sigma)f$, where σ is the classical reflection coefficient as defined earlier on, $\sigma = 1 - K_f\Phi$. The function f is unity for an uncharged membrane, resulting in $\sigma' = \sigma$, which is the classical result for uncharged membranes [8,28]. However, for a charged membranes and a 1:1 salt, we can derive from SF-theory that f is different from unity, as we explain in detail in Supplementary Material. If we assume a good rejection, and a membrane that is at least moderately charged, then $c_p \ll C$, and if we use Eq. (3) to evaluate $c_{T,m}$ on both sides of the membrane, we obtain $f = \sqrt{(C/c_{int})^2 + 1} - C/c_{int}$. This is similar to, but not the same as, Eq. (9–10) in ref. [7]. In a Taylor expansion around $C \sim 0$, the first terms are $f = 1 - C/c_{int} + \mathcal{O}\left((C/c_{int})^2\right)$. This expansion can be used for values of C not larger than 20 % of c_{int}, so it is only a first correction to σ, valid in the limit of low membrane charge. The function f is such that if the classical σ is known (for the uncharged case), that when a membrane charge must be considered, σ' will be larger than σ, closer to 1. So if σ is already close to unity, then σ' will be even closer.

For parameter settings in this study we estimate that σ is already close to unity, and thus σ' will be as well. Thus we set σ' to unity. Furthermore, at high rejections, the osmotic pressure difference, $\Delta\Pi$, can be replaced by Π_{int}, which is the osmotic pressure at a position just outside the membrane on the upstream side. The osmotic pressure can be calculated based on the ideal contribution, $\Pi_{int} = 2c_{int}RT$, but comparison with experiments then showed that Π_{int} is overestimated, and thus the minimum hydrostatic pressure is also overestimated. This minimum pressure is the intersection point with the x-axis of the curve of v_w plotted against ΔP^h, as for instance in Fig. 1C. In Fig. 1C, at c_f = 600 mM this intersection point would be at 30 bar if ideal thermodynamics is assumed, which is too high by about 4 bar to fit the data well. We correct the ideal thermodynamic function by implementing the Bjerrum theory of electrostatic ion-ion interactions, which lowers the osmotic pressure [3]. Bjerrum theory results in a factor by which the ideal osmotic pressure is multiplied to obtain a better estimate of the osmotic pressure, and this factor is $1 - \gamma\sqrt[3]{c_{int}/c_{ref}}$, with $\gamma = 0.0154$ and c_{ref} = 1 mM. At c_{int} = 600 mM, this correction leads to a reduction in the predicted osmotic pressure by 4 bar. Thus, combining all these elements, the expression we use for water flux versus pressure difference in our study is

$$v_w = A\left(\Delta P^{h,\infty} - 2RTc_{int}\left(1 - \gamma\sqrt[3]{c_{int}/c_{ref}}\right)\right). \tag{16}$$

For the data of water flux versus pressure, we now obtain a very good fit of theory to the data for almost all datasets, with one unique value of A that describes water permeability as an intrinsic membrane property.

3. Results and discussion

In this section, the new equation, Eq. (11), is compared with several datasets from literature and newly obtained results. First, data presented in ref. [1] are reanalyzed. In that work a Dupont (FilmTec) SW30-XLE membrane was used that was provided as a flat sheet. These data were also analyzed in ref. [2], and we will do so again. In ref. [2] a best fit was

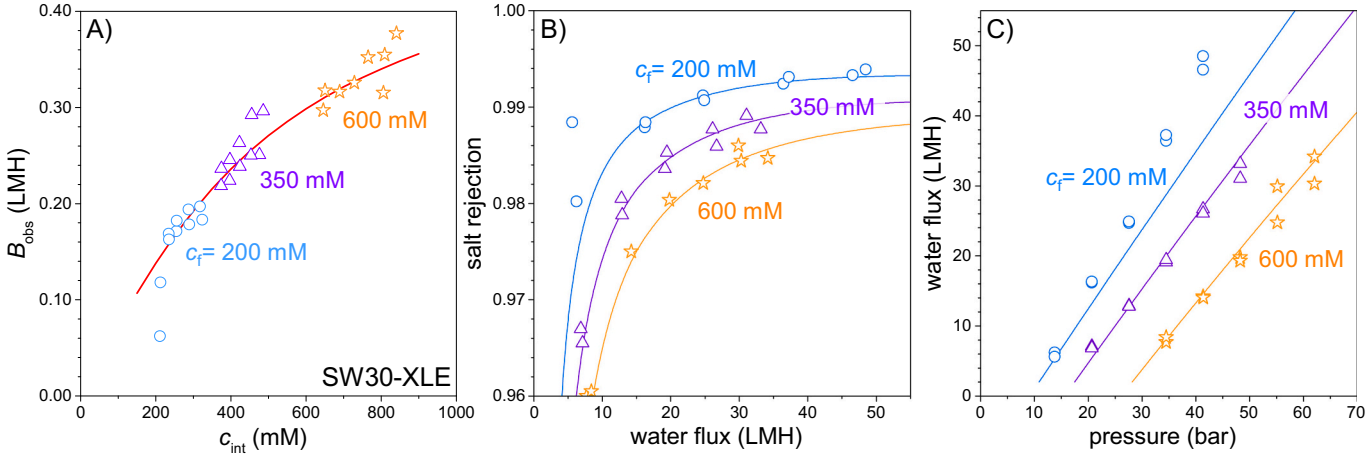

Fig. 1. Data from ref. [1] and theory for RO performance of an SW30-XLE (Dupont) membrane as function of NaCl concentration and transmembrane water flux. Theory based on Eqs. (11), (13), and (15). Parameter values derived from fitting the theoretical curves to the data are A = 1.28 LMH/bar, C = 350 mM, P = 0.52 LMH, and k_{dbl} = 100 LMH. A) Observed salt permeability, B_{obs}, vs. interface concentration, c_{int}; B) rejection, R, vs. water flux, v_w; C) Water flux vs. applied pressure, $\Delta P^{h,\infty}$.

found for the DBL-factor of k_{dbl} = 100 LMH (higher than used in ref. [1]), and that value is used again, because in a plot of B_{obs} versus c_{int} it makes all data fall as much as possible onto a mastercurve, see Fig. 1A. We are of the opinion that this is one of the most accurate methods to find an appropriate value of k_{dbl}, because this method makes use of all data obtained in a certain study. As already concluded in ref. [1], B_{obs} changes with salt concentration by about a factor of two in the concentration range tested. The theoretical line in panel A is based on Eq. (13) and from a fit to the data we derive values of C = 350 mM and P = 0.52 LMH. With these values for C and P, a good fit of theory to data is also found in Fig. 1B where rejection, R, is plotted against transmembrane water flux, v_w. From the data of water flux plotted against pressure, see Fig. 1C, a water permeability of A = 1.28 LMH/bar is derived, lower than values derived in ref. [2] (1.65 LMH/bar) and in ref. [1] (1.85 LMH/bar). We presently arrive at a lower value because the non-ideality of osmotic pressure is included, which reduces the 'opposing force' of osmotic pressure, and thus to fit to the same data, A is reduced.

We next present results of novel experiments, based on a setup and protocol similar to ref. [25] with experiments performed in a commercial test rig (Demcon convergence inspector reverse osmosis pilot system, The Netherlands). The membrane is placed in a stainless steel test cell with a rectangular flow channel that has a height of ~ 3 mm. Inside this empty cavity a sheet of spacer material is placed on top of the membrane. The spacer material is constructed from thin plastic strands that are ~ 0.35 mm in diameter and woven into a single layer forming a pattern with square holes of 1.4 mm × 1.4 mm, with a porosity of the layer around 80 %. This spacer sheet has a thickness of 0.7 mm (twice the diameter of the plastic strands). In the cavity, the spacer is covered by a PMMA plate that fills up all remaining space. So in the experiment, the flow channel has a height of 0.7 mm. The active membrane area (the membrane area through which water and salts will flow) has the same dimensions as the flow channel while the membrane that is placed in the test cell is 1 cm larger on all sides. This membrane is sealed off on the excess area with a rubber seal and is clamped between upper and lower parts of the cell that are screwed together with a torque of 2.5 Nm. Before testing, each membrane coupon was stored in a 25 v% isopropyl alcohol solution for ~ 1 h. Coupons were then gently rinsed with deionized (DI) water and stored in DI water for ~ 1 h. Subsequently, they were placed in the test cells and operated for several hours with DI water at 50 or 60 bar transmembrane pressure. Then pressure was reduced to ~ 10 bar and the cell was run overnight with DI water. Only the next day experiments with salt solutions started. Throughout the experiments, temperature was kept constant at 20–21 °C by cooling the feed solution using a FrioCell (MMM Group, Germany). Transmembrane pressure was changed during each experiment using an automated retentate valve. The active membrane area is rectangular (i.e., has a shorter and longer side) and feed water enters on the short side. Permeate water flow rate, conductivity, and pH are continuously recorded. Salt rejection was calculated based on $R = 1 - \lambda_p/\lambda_f$ with λ_j electrolyte conductivity, with p and f referring to permeate and feed.

We first discuss our experiments in a test cell with a flow channel and active membrane area of 12.7 cm × 19.7 cm = 250 cm^2. We tested a coupon cut from a membrane obtained from disassembling a small RO module of type SW30–2540 (Dupont). The crossflow velocity of feedwater on the high pressure side is 21.5 cm/s. Three feedwater salt concentrations are tested, see Fig. 2. Optimal values to fit theory to data are k_{dbl} = 100 LMH, A = 1.44 LMH/bar, C = 240 mM, and P = 0.49 LMH. Thus the water permeability A is slightly higher than in the dataset of ref. [1] while parameters P and C correspond to the lower rejection than reported in Fig. 1. As Fig. 2B shows, we can fit data well for 200 and 400 mM, but we cannot fit all three datasets at the same time. Because it is more likely that rejection in a certain dataset is inadvertently measured as too low, rather than too high, we give a lower reliability to the dataset at 600 mM in Fig. 1. So we do not use this dataset in the derivation of theoretical parameters. As a consequence of this choice, in the plot of B_{obs} vs. c_{int}, data at 200 and 400 mM are close to a mastercurve for B_{obs} vs. c_{int}, but data at c_f = 600 mM do not. For all datasets, water flux was well described by Eq. (16).

A second new dataset was obtained in a smaller test cell, where we tested feed salinities from 50 mM to 600 mM. The test cell has an A7-sized flow channel and active membrane area, which is 5.0 cm × 7.9 cm, thus the area is 39.5 cm^2. The crossflow velocity of the feedwater on the upstream side is 67.5 cm/s. The membrane, SW30-HRLE (DuPont), was acquired from Sterlitech (Auburn, WA, USA) as flat sheets of 14 cm × 19 cm, from which coupons were cut. As Fig. 3B shows, in this experimental program salt rejection is independent of feed salinity for datasets where c_f is 300 mM or higher, but for lower c_f, rejection increases when c_f goes down. We can accurately describe these data with Eq. (11), and derive for this membrane P = 0.39 LMH and C = 55 mM. The DBL transfer coefficient is 10 % higher than we used in Figs. 1 and 2, thus it is k_{dbl} = 110 LMH. Water permeability is A = 2.2 LMH/bar. The observed salt permeability, B_{obs}, varies by about a factor of 2 between low and high interface concentrations, see Fig. 3A.

Other experiments using brackish water membranes (BW-30 and XLE, both from DuPont, acquired as flat sheets from Sterlitech) resulted in data for salt rejection versus water flux that were 'overlapping' for all feed salt concentration tested, see Fig. S1 (panels D–I) in Supplementary Material, and thus the C-factor to describe these data was small, and in these cases we use C = 0. The salt permeability, $P = B$, was measured as

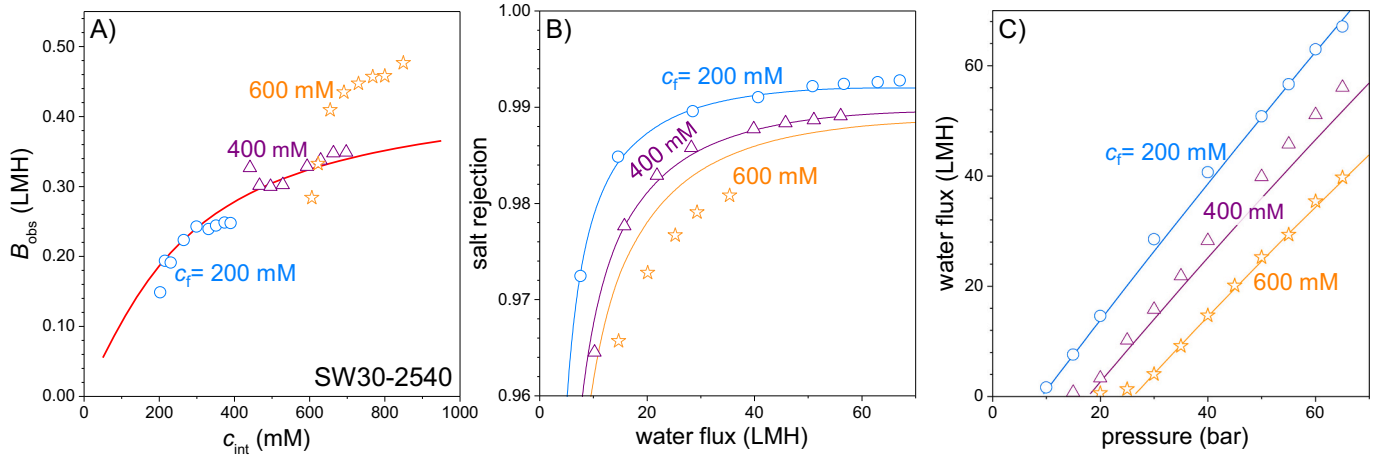

Fig. 2. Data and theory for RO performance, similar to Fig. 1, for a coupon from an SW30-2540 module (Dupont) (A = 1.44 LMH/bar, C = 240 mM, P = 0.49 LMH, k_{dbl} = 100 LMH).

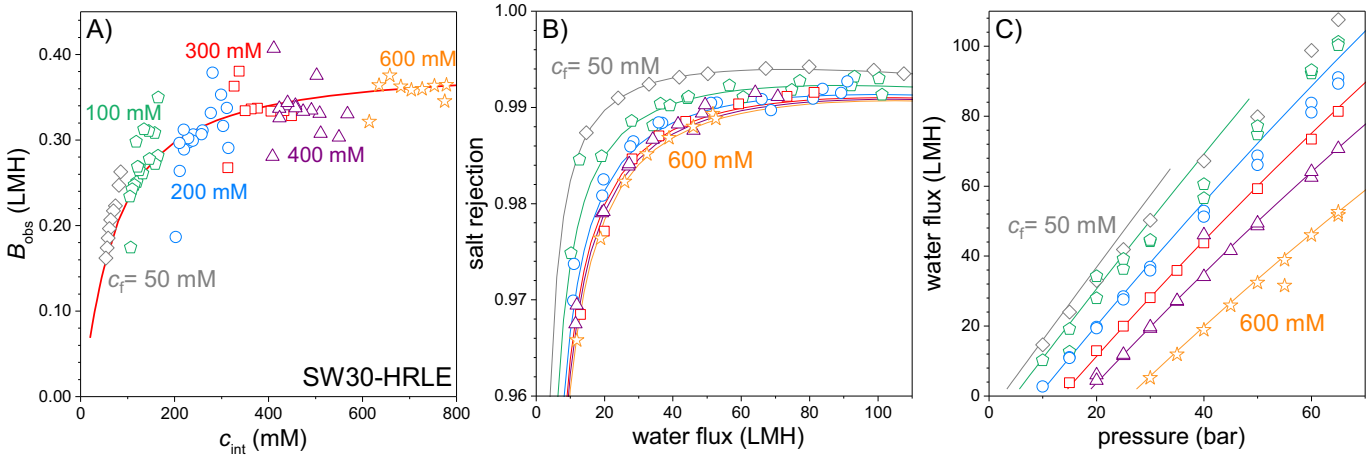

Fig. 3. Data and theory for RO performance, similar to Fig. 1, for an SW30-HRLE flat sheet membrane (Dupont) (A = 2.2 LMH/bar, C = 55 mM, P = 0.39 LMH, k_{dbl} = 110 LMH).

B = 0.72 and 0.95 LMH, respectively. However, to fit both these datasets an excessively high value of k_{dbl} was required ($k_{dbl} \sim 250$ LMH), which seems to imply that there is hardly any effect of the DBL on membrane performance. We do not know why in this experiment we have this outcome (of low to zero apparent membrane charge, and a very high k_{dbl}) that is different from expectations based on the other datasets. Water permeability could be established reliably, at A = 3.3 and 5.0 LMH/bar, respectively.

In Supplementary Material we describe two more datasets from literature [24] that are also without a dependence of rejection and B_{obs} on feed concentration, and thus we have $C \sim 0$ for these two membranes, see Fig. S1. However, in two other datasets from literature [24], see Fig. S2(A–F), an effect of salt concentration on retention is observed, and thus these membranes are expected to be charged. Thus, in some datasets there is evidence of the membrane being charged, while in other datasets membrane charge does not seem to play a role. Why we have this situation, with these two different behaviors, we do not know. If we use an estimate of membrane charge X of a few mM, say X = 10 mM (based on results in ref. [26]), the partition coefficient must be around $\Phi \sim 0.1$ when $C = |X|/2\Phi_i \sim 50$ mM. If we then assume a selective membrane layer thickness of L_m = 100 nm, and take a salt diffusion coefficient of $1.6{\cdot}10^{-9}$ m^2/s, then for a salt permeability $P \sim$ 0.4 LMH, we derive for $K_f\varepsilon$ a value less than $1{\cdot}10^{-4}$, i.e., diffusional rates in the membrane are easily lower than in free solution by a factor 104. Clearly, ions are highly restricted in their motion in the RO TFC toplayer. For electrodialysis membranes, this reduction factor is in the range of 10–50 [27], very much less than in RO membranes.

For charged membranes, salt permeability is described not by one but by two factors, C and P. This situation is unproblematic when the aim of the transport theory is to make theoretical calculations of membrane performance, or for instance module design. However, that we have two intrinsic factors that jointly describe salt permeability, is not optimal when the aim is to compare the rejection of different membranes, or compare between different operational conditions. The most general option is using the full curve of B_{obs} vs c_{int} because this mastercurve defines the performance of a charged membrane for the rejection of a 1:1 salt at all salt concentrations. We can then compare these curves with each other, see Fig. 4A. We can compare the datasets without applying any theory (except deciding on a proper value for k_{dbl}, which can be different for each dataset), or we can compare the theoretical lines for B_{obs}, which were derived as an interpolation of the data.

However, to decide which membrane has the best (i.e., lowest) salt permeability, we ideally compare using a single number. But that requires a decision on the most appropriate value of c_{int}. This choice will

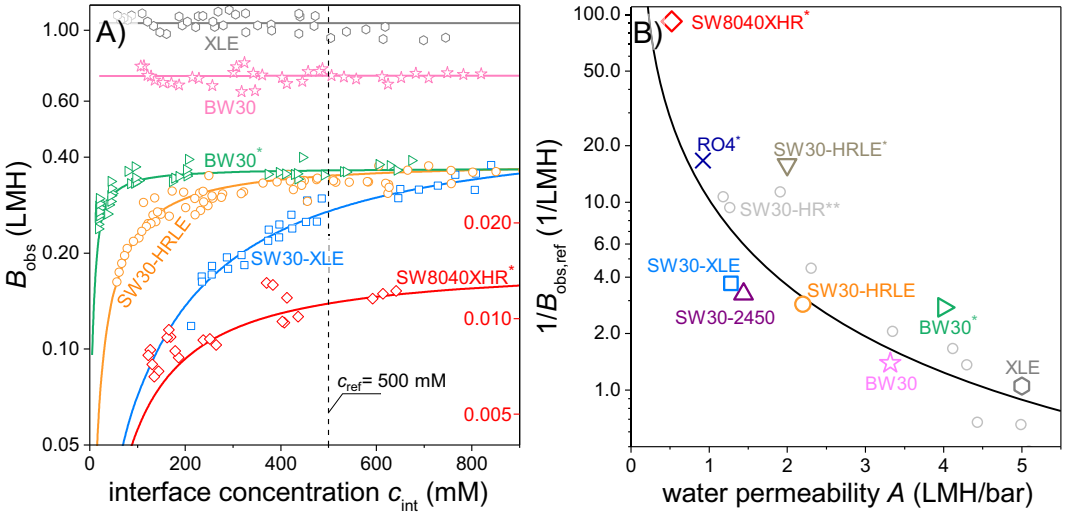

Fig. 4. A) Collection of data and theory for B_{obs} versus c_{int} for selected membranes discussed in this work, each tested at different pressures and salt concentrations. To determine $B_{obs,ref}$ for each membrane, we chose the reference concentration c_{ref} = 500 mM. B). Trade-off diagram containing data for all membranes discussed in this work, plotting an inverse salt permeability for the reference condition, $1/B_{obs,ref}$, against water permeability, A, including also data from ref. [14] (SW30-HR**).

depend on the application of the membrane (brackish water treatment vs. seawater). In this work we choose a reference value of $c_{ref} = 500$ mM (a relevant value for seawater), and if we determine $B_{obs,ref}$ for many membranes at a condition where the interface concentration, c_{int}, is equal to c_{ref}, we can construct a membrane performance tradeoff curve, where we plot the inverse of salt permeability, $1/B_{obs,ref}$, against water permeability, A, for each membrane, see Fig. 4B. Note that we plot $1/B$ versus A, as proposed in ref. [4], which we consider to be a better choice than the standard representation of A/B against A. This is because in setting up trade-off diagrams, the aim is to make the properties plotted against one another, along the two juxtaposed axes, as independent from one another as possible, so there is no good reason to plot A/B instead of $1/B$. We also plot ~ 10 datapoints from ref. [14] which are based on a commercial TFC polyamide RO membrane tested at $c_f = 50$ mM before and after different degrees of chemically treatment to make the membranes more porous, resulting in many datapoints for different A and B. We also plot a fitline which is $B_{obs,ref} = kA^{1.5}$ that we provide just as a guide to the eye ($k = 0.1\sqrt{\text{bar}^3/\text{LMH}}$). It has a lower dependence of B on A than correlations used in literature which for instance are $B \propto A^3$ [14]. This fitline interpolates the best across the data, but it can also be noticed that some membranes tested are about a factor 2 too low in salt rejection (in $1/B_{obs,ref}$), while another has a salt rejection that is a factor 2 better than the fitline. There are many possible explanations for these variations, and we hope that future studies will bring light to this question. Possible explanations are that the membranes that were provided were inherently better or worse (either just the sample, or the specific type), that membrane handling in our laboratories was not optimal, or that small (yet unknown) choices in the testing protocol play a large role (for instance crossflow velocity, pretreatment times).

4. Conclusions

In this work, based on solution-friction theory we presented a novel theoretical equation that comprehensively describes RO membrane performance for a 1:1 electrolyte solution. This equation is valid both for charged and uncharged membranes. We evaluate the equation for experiments at low water recovery. Using this equation we analyze many datasets where a certain membrane is tested at multiple feed salt concentrations, c_f, and multiple applied pressures. Four parameters can be robustly derived from a sufficiently large dataset. When the dataset is large enough, there is the added advantage that all individual datapoints can be checked against one another for internal consistency.

We present many datasets from our own laboratories and from literature, where some membranes have a salt rejection that depends on c_f (comparing at the same water flux) which indicates that in these cases the membrane is charged to a degree that impacts membrane performance. Other membranes do not show a dependence of salt permeability on c_f, indicating that the membrane is uncharged.

Across the datasets that we analyze there are various imperfections such as sub-sets that do not fit the general picture, or parameter values that vary strongly between datasets, such as the DBL mass transfer coefficient. These irregularities can be a natural consequence of the difficulty of measuring RO performance accurately. And they shows the importance to not just do a few experiments with a certain membrane, but perform a sufficiently large study where for the same membrane, rejection is measured at several pressures and salt concentrations, and datasets are checked for internal consistency. We can assign a high reliability to datasets with more reproducibility (repeating the same experiment gives the same result) and when data are more consistent, by which we mean that measured values change gradually or 'smoothly' when input parameters are changed stepwise (i.e., the opposite of data being 'all over the place'). We advocate for other laboratories to undertake similar studies and report their data in the same graphical way as outlined in this work, based on a sufficiently large dataset where the same membrane sample is tested at multiple pressures and feed salinities. From that full dataset values are derived for the intrinsic membrane parameters, A, C, and P, and for k_{dbl}. In this way, a database of measured values is obtained and we can start to understand which protocols provide the most consistent results and which do not. When certain parameter values cannot be rationalized, such as a very high DBL mass transfer coefficient, one can decide to assign a lower reliability to that dataset. We suggest to use pure NaCl for testing, not synthetic seawater, without any other additives in the feedwater.

From a sufficiently large dataset that is internally consistent, one plot that can be constructed is observed salt permeability, B_{obs}, versus interface (membrane) concentration, c_{int}. When (most of) the data collapse into a narrow bandwidth (the mastercurve for B_{obs} vs. c_{int}), then we can reliably read off a value of $B_{obs,ref}$ at a reference concentration, and these values can be compared between different membranes, and plotted in RO membrane performance tradeoff diagrams. We propose a reference concentration of $c_{ref} = 500$ mM. Following this procedure, a large dataset obtained for one particular membrane, leads to one value of water permeability, A, and one value of $B_{obs,ref}$, and we do end up with one and the same membrane tested in a single study having multiple entries in a trade-off diagram.

List of symbols

$\bar{x}$	coordinate, m
x	dimensionless coordinate
L_m	membrane thickness, m
ϕ	dimensionless electrical potential
c	concentration, mol/m^3
$c_\pm$	concentration of cations/anions, mol/m^3
$c_{T,m}$	total concentration, mol/m^3
z	charge number
k	mass transfer coefficient, m/s, or L/m^2/h, i.e., LMH
D	diffusion coefficient, m^2/s
ε	reduction factor due to porosity / tortuosity
K_f	friction factor
v_w	transmembrane water flux, LMH
J	solute flux, mol/(m^2·s)
J_s	salt flux, mol/(m^2·s)
J_{ch}	charge flux, mol/(m^2·s)
X	membrane charge density, mol/m^3
Φ	partition coefficient
σ	reflection coefficient
A	water permeability, LMH/bar
B	salt permeability, LMH
P	transport factor, LMH
C	charge factor, mol/m^3
R	universal gas constant, J/(mol·K)
T	temperature, K
Pe	Péclet number
ΔP	pressure difference, bar
Π	osmotic pressure, bar
γ	constant (=0.0154)

Indices

m	membrane
f, p	feed, permeate
int	membrane interface on the feed side
dbl	diffusion boundary layer
obs	observed
ref	reference

CRediT authorship contribution statement

The manuscript was written through contributions of all authors on

all aspects of the paper: theory, discussion, writing, etc.

All authors have given approval for the final version of the manuscript.

Declaration of competing interest

There are no conflicts of interest.

Data availability

Data will be made available on request.

Acknowledgments

This work was performed in the cooperation framework of Wetsus, European Centre of Excellence for Sustainable Water Technology (www.wetsus.nl). Wetsus is co-funded by the Dutch Ministry of Economic Affairs and Ministry of Infrastructure and Environment, the European Union Regional Development Fund, the Province of Fryslân and the Northern Netherlands Provinces. The authors thank the participants of the research theme Advanced Water Treatment for fruitful discussions and financial support. SP acknowledges financial support from the Polish National Agency for Academic Exchange–Polish Returns grant (BPN/PPO/2021/1/00010).

Appendix A. Supplementary data

Supplementary data to this article can be found online at https://doi.org/10.1016/j.desal.2023.116580.

References

[1] L. Wang, T. Cao, J.E. Dykstra, S. Porada, P.M. Biesheuvel, M. Elimelech, Salt and water transport in reverse osmosis membranes: beyond the solution-diffusion model, Environ. Sci. Technol. 55 (2021) 16665–16675.
[2] P.M. Biesheuvel, J.E. Dykstra, S. Porada, M. Elimelech, New parametrization method for salt permeability of reverse osmosis desalination membranes, J. Membr. Sci. Lett. 2 (2022), 100010.
[3] P.M. Biesheuvel, S. Porada, M. Elimelech, J.E. Dykstra, Tutorial review of reverse osmosis and electrodialysis, J. Membr. Sci. 647 (2022), 120221.
[4] J.R. Werber, A. Deshmukh, M. Elimelech, The critical need for increased selectivity, not increased water permeability, for desalination membranes, ES&T Lett. 3 (2016) 112–120.
[5] Z. Yang, H. Guo, C.Y. Tang, The upper bound of thin-film composite (TFC) polyamide membranes for desalination, J. Membr. Sci. 590 (2019), 117297.
[6] X. Chen, C. Boo, N.Y. Yip, Influence of solute molecular diameter on permeability-selectivity tradeoff of thin-film composite polyamide membranes in aqueous separations, Water Res. 201 (2021), 117311.
[7] O. Kedem, A. Katchalsky, A physical interpretation of the phenomenological coefficients of membrane permeability, J. Gen. Physiol. 45 (1961) 143–179.
[8] K.S. Spiegler, O. Kedem, Thermodynamics of hyperfiltration (reverse osmosis): criteria for efficient membranes, Desalination 1 (1966) 311–326.
[9] O. Kedem, Water and salt transport in hyperfiltration, in: H.K. Lonsdale, H. E. Podall (Eds.), Reverse Osmosis Membrane Research Ch. 1, Plenum Press, New York, 1972, pp. 17–42.
[10] X.L. Wang, T. Tsuru, S.I. Nakao, S. Kimura, The electrostatic and steric-hindrance model for the transport of charged solutes through nanofiltration membranes, J. Membr. Sci. 135 (1997) 19–32.
[11] H. Chmiel, X. Lefebvre, V. Mavrov, M. Noronha, J. Palmeri, Computer simulation of nanofiltration, membranes and processes, in: M. Rieth, W. Schommers (Eds.), Handbook of Theoretical and Computational Nanotechnology 5, Amer. Sci. Publ., 2006, pp. 93–214.
[12] O. Kedem, V. Freger, Determination of concentration-dependent transport coefficients in nanofiltration: defining an optimal set of coefficients, J. Membr. Sci. 310 (2008) 586–593.
[13] E. Hoffer, O. Kedem, Hyperfiltration in charged membranes: the fixed charge model, Desalination 2 (1967) 25–39.
[14] N.Y. Yip, M. Elimelech, Performance limiting effects in power generation from salinity gradients by pressure retarded osmosis, ES&T 45 (2011) 10273–10282.
[15] A.E. Yaroshchuk, Rejection of single salts versus transmembrane volume flow in RO/NF: thermodynamic properties, model of constant coefficients, and its modification, J. Membr. Sci. 198 (2002) 285–297.
[16] S. Bason, O. Kedem, V. Freger, Determination of concentration-dependent transport coefficients in nanofiltration: experimental evaluation of coefficients, J. Membr. Sci. 326 (2009) 197–204.
[17] W. Pusch, Determination of transport parameters of synthetic membranes by Hyperfiltration experiments part II: membrane transport parameters independent of pressure and/or pressure difference, Ber. Bunsenges. Phys. Chemie 81 (1977) 854–864.
[18] G. Jonsson, Overview of theories for water and solute transport in UF/RO membranes, Desalination 35 (1980) 21–38.
[19] R. Levenstein, D. Hasson, R. Semiat, Utilization of the Donnan effect for improving electrolyte separation with nanofiltration membranes, J. Membr. Sci. 116 (1996) 77–92.
[20] J.M.M. Peeters, J.P. Boom, M.H.V. Mulder, H. Strathmann, Retention measurements of nanofiltration membranes with electrolyte solutions, J. Membr. Sci. 145 (1998) 199–209.
[21] W.R. Bowen, J.S. Welfoot, Modelling the performance of membrane nanofiltration – critical assessment and model development, Chem. Eng. Sci. 57 (2002) 1121–1137.
[22] V.M. Starov, N.V. Churaev, Separation of electrolyte solutions by reverse osmosis, Adv. Colloid Interf. Sci. 43 (1993) 145–167.
[23] C. Bartels, R. Franks, S. Rybar, M. Schierach, M. Wilf, The effect of feed ionic strength on salt passage through reverse osmosis membranes, Desalination 184 (2005) 185–195.
[24] B. Blankert, K.Th. Huisman, F.D. Martinez, J.S. Vrouwenvelder, C. Picioreanu, Are commercial polyamide seawater and brackish water membranes effectively charged? J. Membr. Sci. Lett. 2 (2022), 100032.
[25] M. Pranić, E.M. Kimani, P.M. Biesheuvel, S. Porada, Desalination of complex multi-ionic solutions by reverse osmosis at different pH values, temperatures, and compositions, ACS Omega 6 (2021) 19946–19955.
[26] E. Kimani, M. Pranić, S. Porada, A.J.B. Kemperman, I.I. Ryzhkov, W.G.J. van der Meer, P.M. Biesheuvel, The influence of feedwater pH on membrane charge ionization and ion rejection by reverse osmosis: an experimental and theoretical study, J. Membr. Sci. 660 (2022), 120800.
[27] S. Ozkul, J.J. van Daal, N.J.M. Kuipers, R.J.M. Bisselink, H. Bruning, J.E. Dykstra, H.H.M. Rijnaarts, Transport mechanisms in electrodialysis: the effect on selective ion transport in multi-ionic solutions, J. Membrane Sci. 665 (2022), 121114.
[28] O. Kedem, A. Katchalsky, Thermodynamic analysis of the permeability of biological membranes to non-electrolytes, Biochim. Biophys. Acta 27 (1958) 229–246.